Biomacromolecules

pubs.acs.org/Biomac Article

Nonionic Water-Soluble Oligo(ethylene glycol)-Modified Polypeptides with a β-Sheet Conformation

Published as part of Biomacromolecules virtual special issue "Peptide Materials".

Xiaodong Jing,[¶] Zhen Zhu,[¶] Shuo Wang, Jiaqi Xin, Haisen Zhou, Letian Wang, Huimin Tong, Chenhui Cui, Yanfeng Zhang, Fei Sun, Lijiang Yang,* Yiqin Gao,* and Hua Lu*

Cite This: *Biomacromolecules* 2024, 25, 5343−5351 Read Online

ABSTRACT: The secondary structures of polypeptides, such as an α-helix and a β-sheet, often impart specific properties and functions, making the regulation of their secondary structures of great significance. Particularly, water-soluble polypeptides bearing a β-sheet conformation are rare and challenging to achieve. Here, a series of oligo(ethylene glycol)-modified lysine *N*-carboxylic anhydrides (^{EGm}K-NCA, where m = 1−3) and the corresponding polymers $^{EGm}K_n$ are synthesized, with urethane bonds as the linker between the side-chain EG and lysine. The secondary structure of $^{EGm}K_n$ is delicately regulated by both m and n, the length (number of repeating units) of EG and the degree of polymerization (DP), respectively. Among them, $^{EG2}K_n$ adopts a β-sheet conformation with good water solubility at an appropriate DP and forms physically cross-linked hydrogels at a concentration as low as 1 wt %. The secondary structures of $^{EG1}K_n$ can be tuned by DP, exhibiting either a β-sheet or an α-helix, whereas $^{EG3}K_n$ appears to a adopt pure and stable α-helix with no dependence on DP. Compared to previous works reporting EG-modified lysine-derived polypeptides bearing exclusively an α-helix conformation, this work highlights the important and unexpected role of the urethane connecting unit and provides useful case studies for understanding the secondary structure of polypeptides.

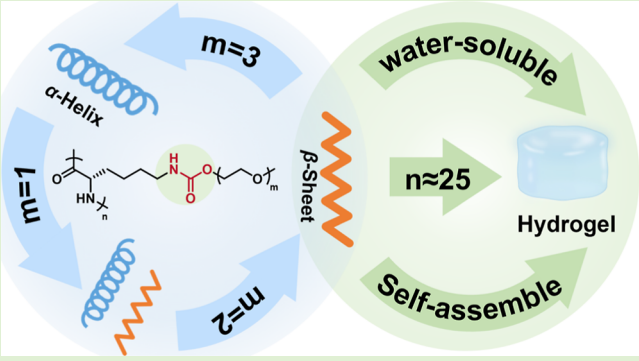

INTRODUCTION

Proteins play many important roles in virtually every aspect of living processes, often through their ordered secondary structures such as the α-helix, β-sheet, and turns.[1−4] To manipulate the secondary structures and better understand the relationship between the secondary structures and biological functions of proteins, synthetic polypeptides with specific conformations are ideal model systems.[5−7] One commonly used method to prepare polypeptides is the ring-opening polymerization (ROP) of amino acid *N*-carboxylic anhydrides (NCAs). By designing NCAs bearing different side chains and/or through postpolymerization modifications, novel polypeptides with rich functionalities have been created, which often exhibit fascinating material properties and biological functions depending on their distinctive secondary structures.[8−23]

Water-soluble polypeptides bearing certain secondary structures are desirable for specific biological applications. While introducing charges into the amino acid residues has been a common strategy for enhanced water solubility, the conformation of ionic polypeptides such as poly(L-glutamic acid) and poly(L-lysine), however, can be easily disrupted by pH, temperature, and salt concentration, rendering a random coil rather than a conformation α-helix under physiological conditions.[24,25] Moreover, the electrostatic interactions of charged groups often cause aggregation and precipitation of ionic polypeptides and/or nonspecific interactions with other biomolecules, making them unsuitable for some specific scenarios. In this regard, the introduction of nonionic oligo(ethylene glycol) (EG_m, where m = the number of repeating units) with good water solubility and excellent antibiofouling ability into the amino acid residue of polypeptides has become a widely adopted alternative strategy.[26−28] Deming pioneered the EG_m-modified polylysine via an amide bond between carboxyl-modified EG_m and the ε-amine residue of lysine, affording neutral, water-soluble polypeptides with a characteristic α-helical conformation in 1999 (Figure 1a).[29] Similarly, Klok et al. prepared EG_m-

Received: June 4, 2024
Revised: June 18, 2024
Accepted: June 20, 2024
Published: July 13, 2024

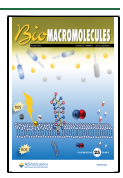

https://doi.org/10.1021/acs.biomac.4c00759
Biomacromolecules 2024, 25, 5343−5351

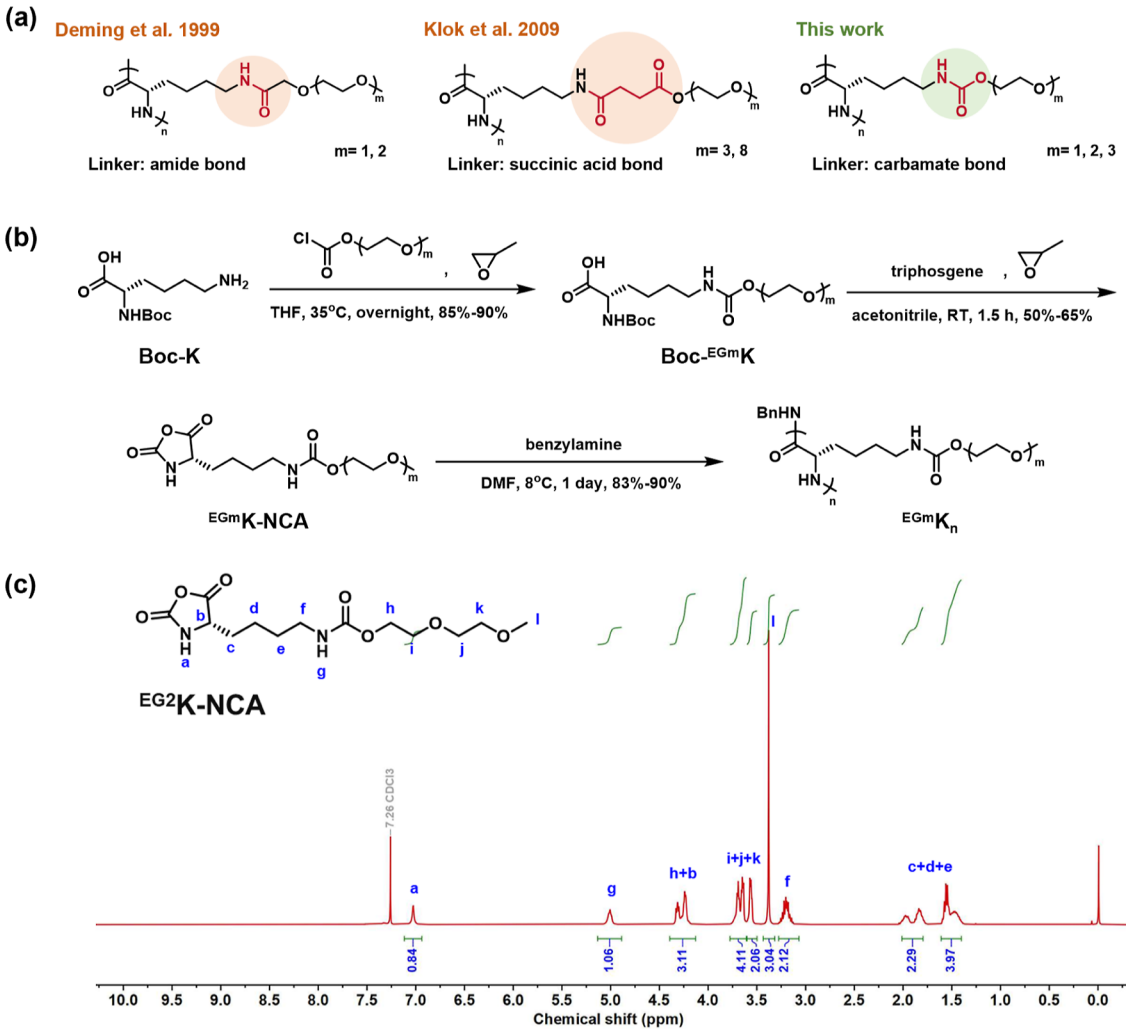

Figure 1. (a) Comparison of the polymer structures used in this study with previous works. (b) Synthesis of ^{EGm}K-NCA monomers and the corresponding polypeptides $^{EGm}K_n$; (c) ^{1}H NMR spectrum of ^{EG2}K-NCA in $CDCl_3$.

modified polylysine using succinic acid as a linker to connect EG_m and the ε-amine of lysine, which also exhibits an α-helical structure conformation[30] and possesses excellent antifouling properties on substrate surfaces (Figure 1a). Moreover, EG_m-functionalized poly-L-glutamate,[13,14,31,32] poly-L-cysteine,[33,34] poly-L-serine,[35,36] and other polypeptides[37−39] have also been explored.

Mounting evidence has shown that the secondary structures of polypeptides are generally determined by the amino acids used, which have their own tendency to form specific secondary structures. For example, glutamic acid and lysine themselves have a strong tendency to form α-helices, and the secondary structures of the above-mentioned polymers are also predominantly α-helices.[40] Similarly, serine and cysteine have a high tendency to form β-sheets, and the secondary structures of polypeptides derived from these two amino acids are often β-sheets. Of note, reports on water-soluble β-sheet polypeptides are extremely rare compared with those with an α-helical conformation.[35,41,42] Meanwhile, the length of EG_m and the linker between EG_m and amino acids have not shown significant influence on the secondary structure of polypeptides.

Here, we report a series of EG_m-modified polylysines, denoted as $^{EGm}K_n$ (n = monomer/initiator feeding ratio), with tunable secondary structures depending highly on not only the length of EG_m and the degree of polymerization (DP) but also the linker. It should be emphasized that, different from the early works of Deming and Klok connecting EG_m and lysine with amide bonds (Figure 1a), urethane bonds are used to connect EG_m and the ε-amine of lysine in this work. Among all the $^{EGm}K_n$ polymers obtained, $^{EG2}K_{25}$ is particularly interesting in that it exhibits a β-sheet conformation that is rare for lysine-based polypeptides and possesses good water solubility greater than 30 mg/mL. Moreover, $^{EG2}K_{25}$ was capable of forming transparent, physically cross-linked hydrogels at low concentrations of 1−7% and remaining stable across a wide temperature range of 4−80 °C. $^{EG1}K_n$ is found to show limited water solubility with a mixed β-sheet and α-helical conformation relying on DP. In contrast, $^{EG3}K_n$ are highly water-soluble and adopt exclusively an α-helix regardless of the DP. Moreover, $^{EG1}K_n$ and $^{EG2}K_n$ show little temperature sensitivity, whereas $^{EG3}K_n$ exhibit a typical lower critical solution temperature (LCST).

■ EXPERIMENTAL SECTION

Synthesis of ^{EG2}K-NCA. To a 500 mL flask were added 2-(2-methoxyethoxy) ethanol (20.00 g, 166.46 mmol, 1.0 equiv), bis(trichloromethyl) carbonate (17.29 g, 58.26 mmol, 0.35 equiv),

https://doi.org/10.1021/acs.biomac.4c00759
Biomacromolecules 2024, 25, 5343−5351

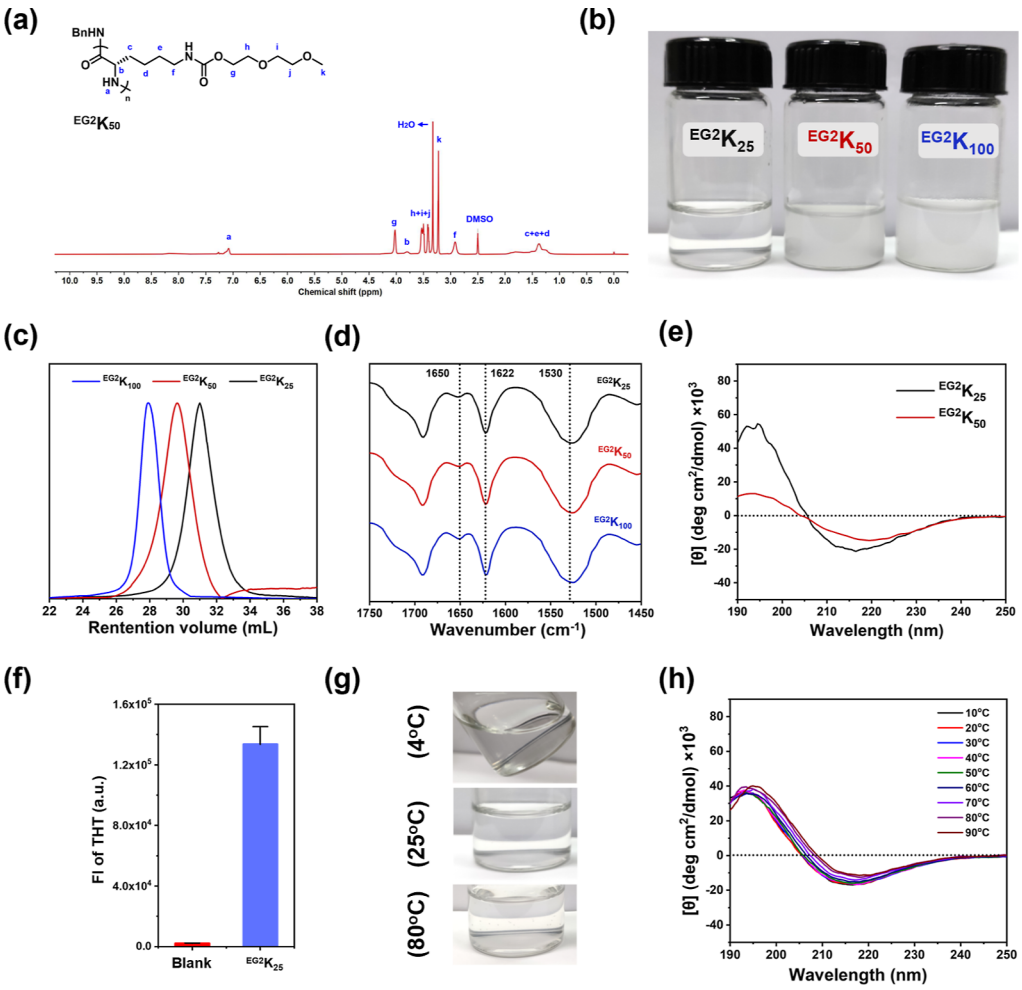

Figure 2. (a) ^{1}H NMR spectrum of $^{EG2}K_{50}$; (b) photographs of $^{EG2}K_n$ dissolved/dispersed in deionized water (2.0 mg/mL); (c) SEC traces of $^{EG2}K_n$; (d) overlay of the FT-IR spectra of $^{EG2}K_n$ in the solid state; (e) CD spectra of the $^{EG2}K_n$ polymers in deionized water (0.3 mg/mL); (f) fluorescence intensity of ThT-stained $^{EG2}K_{25}$; (g) photographs of the dissolved $^{EG2}K_{25}$ in deionized water (2.0 mg/mL) at 4, 25, and 80 °C, respectively; (h) CD spectra of $^{EG2}K_{25}$ at different temperatures between 10 and 90 °C (0.3 mg/mL).

and THF (AR, 200 mL) sequentially. Triethylamine (23.14 mL, 166.46 mmol, 1.0 equiv) was then added dropwise to the reaction system. The temperature of the reaction was controlled by a water bath at 20 °C for 3 h. After filtration, a light-yellow liquid was obtained by a rotavapor under reduced pressure. The product obtained, namely, 2-(2-methoxyethoxy)ethyl carbonochloridate, was redissolved in THF (AR, 500 mL) (1 L flask) and N^{α}-(*tert*-butoxycarbonyl)-L-lysine (36.65 g, 148.80 mmol, 1.0 equiv) and propylene oxide (PO, 31.7 mL, 446.39 mmol, 3.0 equiv) were added to the solution in sequence, and the reaction was heated (35 °C) overnight in a sealed system. The product was concentrated and mixed with deionized water (500 mL). After adjusting the pH to ~8.0, a light-yellow transparent system was obtained. After extraction with ethyl acetate four times, the pH was adjusted to 3.0 with HCl. The product was then transferred to ethyl acetate. After rotavaporization under reduced pressure, a light-yellow viscous liquid was obtained. The product can be used for the synthesis of ^{EG2}K-NCA without further purification.

Boc-^{EG2}K−OH (8.0 g, 20.38 mmol, 1.0 equiv) was first dissolved in acetonitrile (AR, 60 mL), and PO (7.13 mL, 101.92 mmol, 5.0 equiv) and bis(trichloromethyl) carbonate (4.00 g, 13.65 mmol, 0.67 equiv) were added to the open system in sequence, and a water bath was used to control the temperature of the reaction and avoid a violent reaction. The reaction was completed in ~2 h. The solvent was removed by evaporation under reduced pressure. The crude product (solvent-free) required further purification using column chromatography to obtain a viscous pure product (PE/EA = 5:1 ~EA).

Synthesis of $^{EG2}K_n$. All polymerizations studied used benzylamine as the initiator to initiate NCA ROP. Specifically, $^{EG2}K_{25}$−NCA (2.0 g, 6.28 mmol, 25 equiv) was first dissolved in 5.0 mL of DMF at 8 °C, and the corresponding amount of benzylamine (26.92 mg, 0.25 mmol, 1.0 equiv) was added to the system. The reaction was carried out under vacuum for at least 24 h, and the product was dialyzed (MWCO 7000) in deionized water for 48 h and then freeze-dried. The feeding ratio of monomer to initiator was used to determine the nomenclature of the polymer, and the final product was named $^{EG2}K_{25}$. $^{EG2}K_{50}$ and $^{EG2}K_{100}$ were prepared according to the same method. The corresponding monomer and initiator inputs were ^{EG2}K-NCA (2.0 g, 6.28 mmol, 50 equiv), benzylamine (13.46 mg, 0.125 mmol, 1.0 equiv); ^{EG2}K-NCA (2.0 g, 6.28 mmol, 100 equiv), benzylamine (6.73 mg, 0.063 mmol, 1.0 equiv).

RESULTS AND DISCUSSION

A series of EG_m-modified L-lysine connected via urethane bonds were successfully synthesized and termed ^{EGm}K-NCA (m = 1, 2, 3), see the scheme in Figure 1b. Taking ^{EG2}K-NCA as an example, (2-(2-methoxyethoxy) ethanol) was first converted into chloroformate and further reacted with Boc-Lys to generate Boc-^{EG2}K. By adapting the recently developed NCA synthesis method of adding PO as an additive,[43,44] Boc-^{EG2}K was cyclized with triphosgene to afford ^{EG2}K-NCA with a yield of ~60% without the use of stringently anhydrous

https://doi.org/10.1021/acs.biomac.4c00759
Biomacromolecules 2024, 25, 5343−5351

Table 1. Molecular Weight, Dispersity, Secondary Structure, and Water Solubility Characterization of $^{EGm}K_n$

entry[a]	$[M]_0/[I]_0$[a]	sample[a]	Mn (kDa)[b]	Đ[b]	DP[b]	yield (%)	secondary structure[c]	water solubility[d]
1	25	$^{EG2}K_{25}$	5.9	1.14	22	89%	β-sheet	+
2	50	$^{EG2}K_{50}$	17.0	1.26	62	83%	β-sheet	−
3	100	$^{EG2}K_{100}$	34.6	1.13	126	83%	β-sheet	−
4	25	$^{EG1}K_{25}$	7.6	1.19	27	87%	α-helix/β-sheet	−
5	50	$^{EG1}K_{50}$	19.1	1.26	69	85%	α-helix	−
6	100	$^{EG1}K_{100}$	33.6	1.13	122	84%	α-helix	−
7	25	$^{EG3}K_{25}$	10.2	1.34	32	90%	α-helix	++
8	50	$^{EG3}K_{50}$	25.2	1.21	79	87%	α-helix	++
9	100	$^{EG3}K_{100}$	41.7	1.03	131	85%	α-helix	++

[a]Conditions: $[M]_0$ = 1.0 M, initiator: I = benzylamine, polymerization in DMF at 8 °C for 1 day. [b]Determined by SEC (DMF with 0.1 M LiBr) with determined dn/dc values (entries 1−3: 0.0518; entries 4−6: 0.0846; entries 7−9: 0.0531). [c]Determined by FT-IR and CD spectroscopy. [d]Samples are visually tested at a target concentration of 2.0 mg/mL in deionized water.

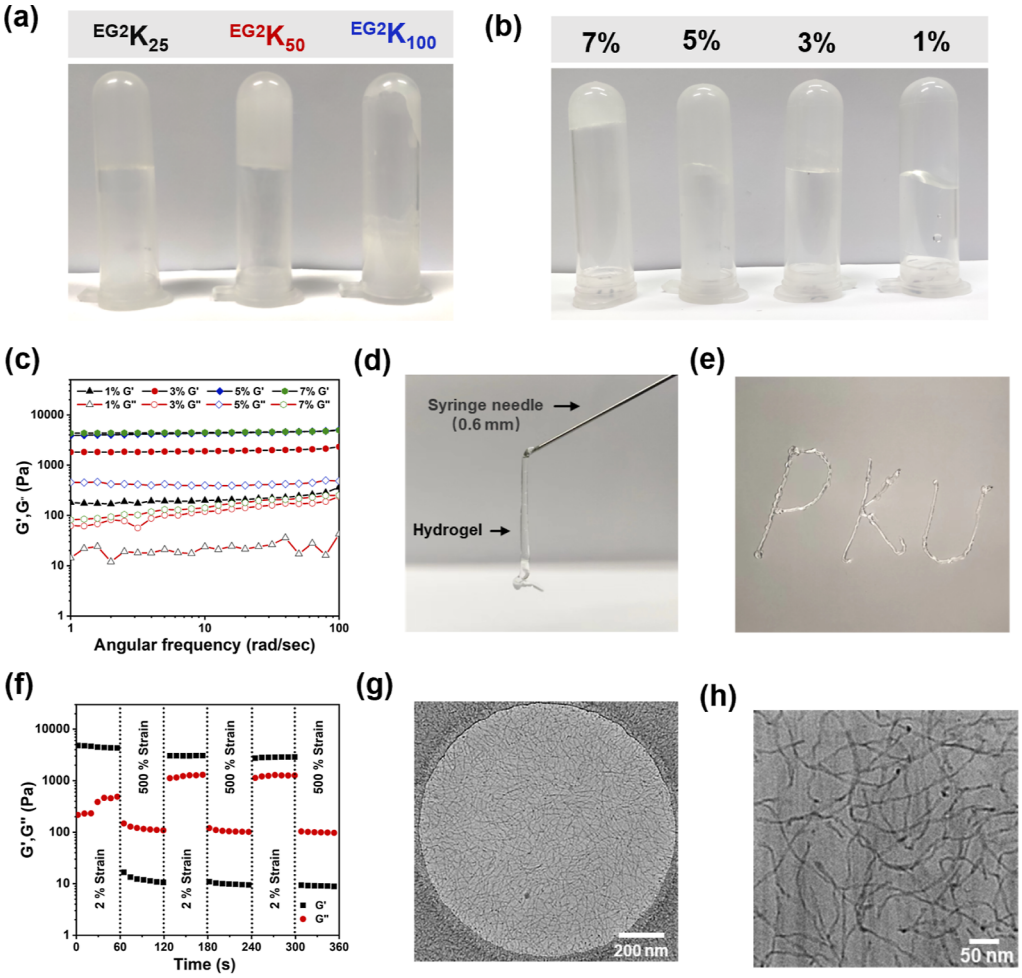

Figure 3. (a) Photographs of the inverse-tube testing of different $^{EG2}K_n$ samples at a concentration of 50 mg/mL (5 wt %); (b) photographs of $^{EG2}K_{25}$ at concentrations from 1 to 7 wt %; (c) rheological tests of the $^{EG2}K_{25}$ hydrogels at different concentrations; (d) photograph demonstrating the extrusion of the 1 wt % $^{EG2}K_{25}$ hydrogel through a syringe (0.6 mm) and (e) generating a "PKU" pattern after the extrusion; (f) rheological properties of the 5 wt % $^{EG2}K_{25}$ hydrogel under alternating strains between 2 and 500%; (g) full-field and (h) magnified cryo-TEM images of $^{EG2}K_{25}$ solution.

conditions and dry solvents. ^{EG1}K-NCA and ^{EG3}K-NCA were prepared by the same route (Figures S1 and S2), with yields of approximately 60 and 55%, respectively. The high purity of ^{EGm}K-NCA was collectively confirmed by various characterizations including proton and carbon nuclear magnetic resonance (^{1}H and ^{13}C NMR) spectroscopy, Fourier-transform infrared (FT-IR) spectroscopy, and electrospray ionization mass spectrometry (ESI-MS) (Figures 1c and S3−S10).

Subsequently, the ROP of ^{EG2}K-NCA in DMF was initiated using benzylamine at different monomer-to-initiator ratios ($[M]_0/[I]_0$ = 25, 50, 100) at 8 °C. ^{1}H NMR spectroscopy confirmed the successful generation of the polymers $^{EG2}K_n$ (Figure 2a). The obtained three polymers (namely, $^{EG2}K_{25}$,

https://doi.org/10.1021/acs.biomac.4c00759
Biomacromolecules 2024, 25, 5343−5351

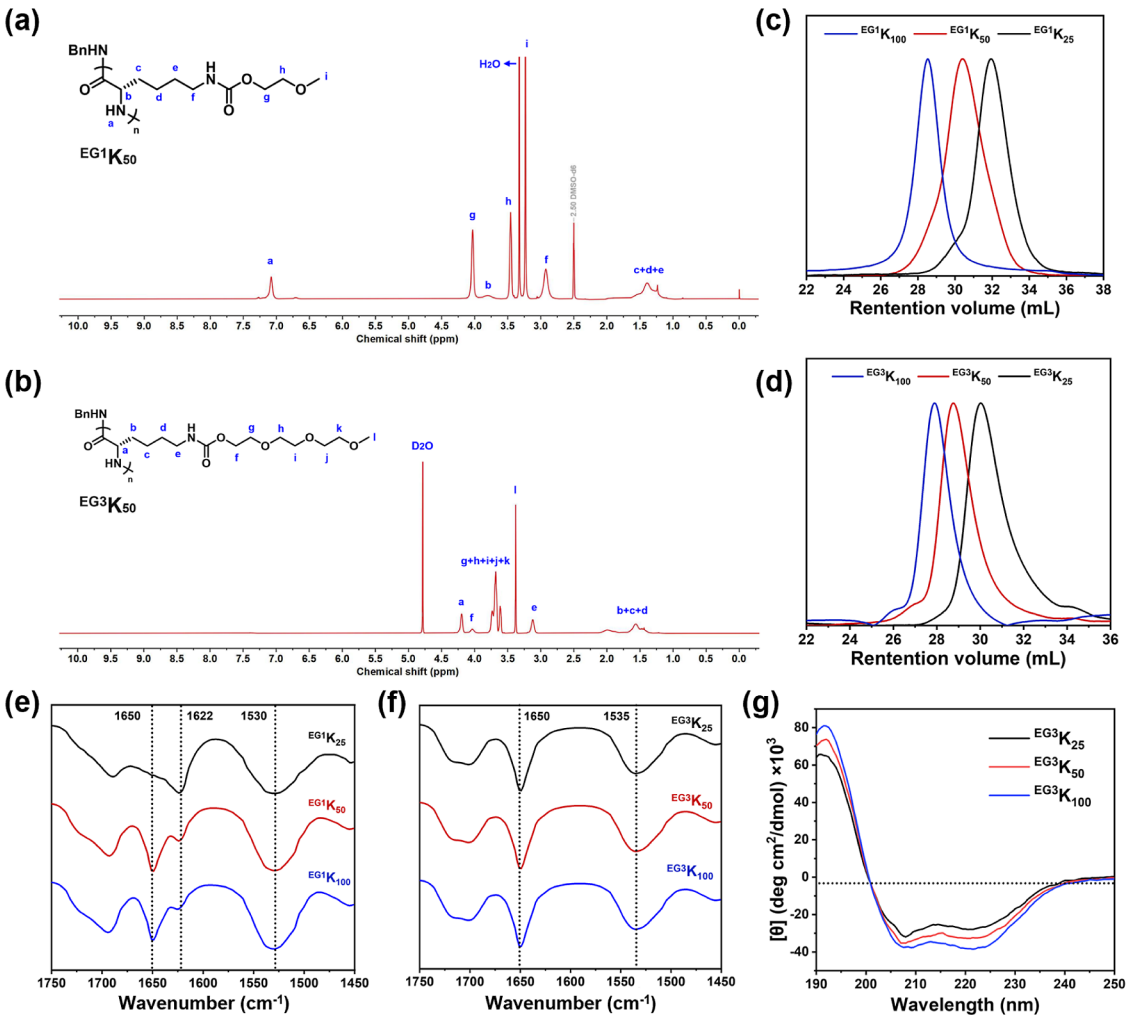

Figure 4. ^{1}H NMR spectra of (a) $^{EG1}K_{50}$ and (b) $^{EG3}K_{50}$; overlay of the SEC curves of (c) $^{EG1}K_n$ and (d) $^{EG3}K_n$; overlay of the FT-IR spectra of (e) $^{EG1}K_n$ and (f) $^{EG3}K_n$ in the solid state; (g) CD spectra of $^{EG3}K_n$ in deionized water (0.3 mg/mL); (h) overlay of the FT-IR spectra of $^{EG2}K_{25}$ and $^{EG3}K_{25}$ in the solid state; (i) conjecture regarding the interplay of side-chain interactions in polymers in aqueous solutions.

$^{EG2}K_{50}$, and $^{EG2}K_{100}$, respectively) all displayed considerable solubility in DMF, and remarkably, $^{EG2}K_{25}$ showed good water solubility above 30 mg/mL (Figure 2b). Consistent with other reports,[45] the solubility in water of all $^{EG2}K_n$ samples decreased with greater DPs ($^{EG2}K_{50}$: 0.2 mg/mL; $^{EG2}K_{100}$: insoluble) (Figure 2b). Size exclusion chromatography (SEC) depicted relatively symmetrical and unimodal peaks for all three polymers (Figure 2c), and the dispersity ($Đ$) ranged from 1.13 to 1.26 (entries 1−3, Table 1). The obtained number-average molecular weight (M_n) values of $^{EG2}K_n$ were relatively close to their expected M_n (entries 1−3, Table 1), indicating good control of the polymerization. The FT-IR spectra of the $^{EG2}K_n$ polymers in the solid state showed major amide I and amide II peaks at 1622 and 1530 cm^{-1}, respectively, which were characteristic β-sheet signals. In addition, a weak absorption amide I peak at 1650 cm^{-1} was observed (Figure 2e), indicating that a minor α-helix coexisted with a predominantly β-sheet conformation for $^{EG2}K_n$. Moreover, the secondary structure of $^{EG2}K_n$ appeared to have no obvious correlation with the DP. The circular dichroism (CD) spectra of both $^{EG2}K_{25}$ and $^{EG2}K_{50}$ showed a negative peak at 216 nm (typical β-sheet signal) in deionized water, confirming the results of the FT-IR. Of note, the weaker signal of $^{EG2}K_{50}$ relative to $^{EG2}K_{25}$ was attributed to its poor solubility in water. Staining of $^{EG2}K_{25}$ with thioflavin T (ThT),[46] a β-sheet indicator, showed strong fluorescence and thus further verified the above conclusion (Figure 2f). It should be pointed out that $^{EG2}K_{25}$ switched the original α-helical conformation tendency of L-lysine to yield a neutral, water-soluble β-sheet polymer, which is fairly rare. Interestingly, the solubility of $^{EG2}K_{25}$ seemed unchanged in the range of 10−90 °C (Figure 2g), which was different from previous examples where EG_m-containing polypeptides were often reported to give thermal responsiveness.[47−49] In addition, the solubility and secondary structure of $^{EG2}K_{25}$ were not affected at varying temperatures (Figure 2h) and pH (Figure S10).

We reasoned that $^{EG2}K_{25}$ had the potential to form hydrogels because of its good water solubility and β-sheet secondary structure, which normally promotes strong self-assembly of polypeptides via strong interchain hydrogen bonding. Small-angle X-ray scattering examination of $^{EG2}K_{25}$ in solid form gave characteristic peaks relating to self-assembled structures, supporting the notion of possible microphase separation (Figure S11). Moreover, when dissolving $^{EG2}K_{25}$ at a concentration of 0.8 mg/mL, dynamic light scattering (DLS) gave a strong signal corresponding to self-assembled nanoparticles with a diameter of approximately 165 nm (Figure S12). A transparent hydrogel was obtained at 5 wt % of $^{EG2}K_{25}$,

https://doi.org/10.1021/acs.biomac.4c00759
Biomacromolecules 2024, 25, 5343−5351

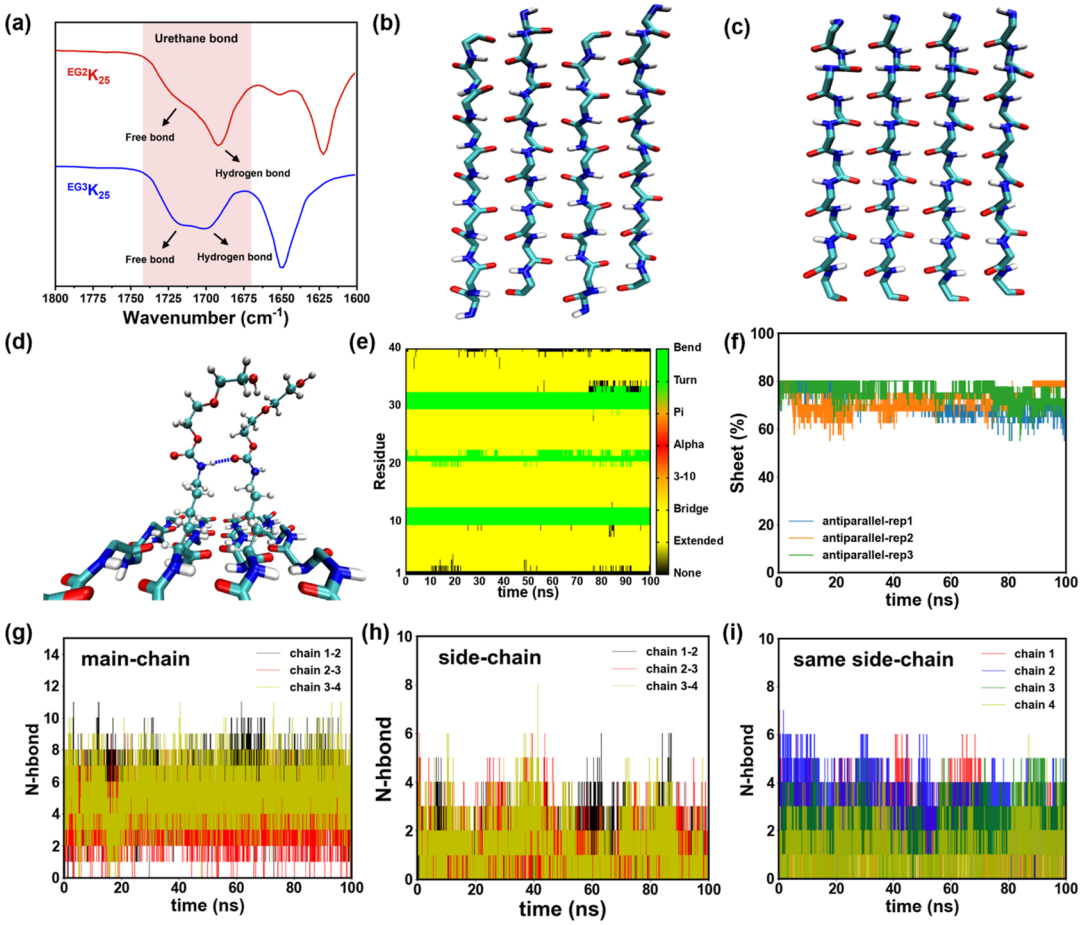

Figure 5. (a) FT-IR spectra of the side-chain urethane bonds of $^{EG2}K_{25}$ and $^{EG3}K_{25}$. The backbone of the $^{EG2}K_n$ antiparallel β-sheet (b) and parallel β-sheet (c). From left to right, they represent chain 1, chain 2, chain 3, and chain 4, with the corresponding residue IDs being 1−10, 11−20, 21−30, and 31−40. (d) Schematic diagram of side-chain hydrogen bonds. Side chains are represented by CPK, with oxygen atoms in red and hydrogen atoms in white. Hydrogen bonds between oxygen and hydrogen atoms are indicated by blue dashed lines. (e) Secondary structure evolution of the $^{EG2}K_n$ β-sheet over simulation time. (f) β-sheet content of the $^{EG2}K_n$ β-sheet versus simulation time. (g) Total number of hydrogen bonds between the main chains of the $^{EG2}K_n$ β-sheet versus simulation time. The total number of hydrogen bonds on the side chains between different chains (h) and within the same chain (i) of the $^{EG2}K_n$ β-sheet versus simulation time.

while $^{EG2}K_{50}$ formed an opaque hydrogel at the same concentration (Figure 3a). Remarkably, when the concentration of the polymer was reduced to 1%, $^{EG2}K_{25}$ still maintained the gel state (Figure 3b). Rheological tests showed greater storage moduli (G') than the loss moduli (G'') of $^{EG2}K_{25}$ at different concentrations, another indication of the gel state.[50,51] The G' of the 5% $^{EG2}K_{25}$ hydrogel reached approximately 4000 Pa, similar to the same hydrogel with a polymer content of 7% (Figure 3c). As a physically cross-linked gel, the $^{EG2}K_{25}$ sample was injectable, extrudable with a 0.6 mm needle (Figure 3d), and then recoverable to the gel state (Figure 3e). The $^{EG2}K_{25}$ hydrogel also exhibited a reversible gel-to-solution transition under alternating strains (2−500%), showcasing its excellent self-healing ability (Figure 3f). Cryo-transmission electron microscopy (Cryo-TEM) of $^{EG2}K_{25}$ in aqueous solution exhibited a dense network of polymeric fibers with the average length exceeding 1200 nm and a diameter of ∼4.7−5.5 nm (Figure 3g−h).

Knowing that the length, or number of repeating units, of EG_m would likely affect the hydrophilicity and secondary structures of the polypeptides,[52,53] we next prepared two series of polypeptides by varying the length of EG_m, namely, $^{EG1}K_n$ and $^{EG3}K_n$ (Figure 1). The ^{1}H NMR spectra in Figure 4a,b demonstrated the successful preparation of $^{EG1}K_n$ and $^{EG3}K_n$. The SEC curves of $^{EG1}K_n$ and $^{EG3}K_n$ are shown in Figure 4c,d, with $Đ$ between 1.03 and 1.34 and controlled M_n (entries 4−9, Table 1). FT-IR spectra indicated that $^{EG1}K_n$ in the solid state had mixed α-helical and β-sheet secondary structures depending on the DP, with $^{EG1}K_{50}$ and $^{EG1}K_{100}$ mainly adopting an α-helix, while $^{EG1}K_{25}$ exhibiting a β-sheet (Figure 4e). The underlying reason for this DP-dependent secondary structure is still under investigation. CD spectroscopy of $^{EG1}K_n$ in water was attempted but failed, mainly due to the extremely poor water solubility of the samples (Figure S13). A similar synthetic route was used to prepare $^{EG3}K_m$ samples with different degrees of polymerization (entries 7−9, Table 1). In contrast, FT-IR spectra of all $^{EG3}K_n$ showed strong absorption peaks at 1650 cm^{-1} (amide I) and 1535 cm^{-1} (amide II) but no peak at 1622 cm^{-1}, indicating exclusively an α-helical conformation (Figure 4f). The CD spectrum in deionized water also showed that the secondary structure of $^{EG3}K_n$ was an α-helix with a helicity of approximately 78%, which was consistent with the results obtained by FT-IR (Figure 4g). $^{EG3}K_n$ all had considerably improved water solubility compared to that of $^{EG2}K_n$ and $^{EG2}K_n$ for the increased EG_m side-chain length (Figure S14). Notably, $^{EG3}K_{25}$ showed typical LCST

https://doi.org/10.1021/acs.biomac.4c00759
Biomacromolecules 2024, 25, 5343−5351

properties at ∼50 °C conferred by the EG_m fragment (Figure S15).

To understand why $^{EG2}K_{25}$ and $^{EG3}K_{25}$ adopted different secondary structures, we focused on analyzing and comparing the FT-IR spectra of $^{EG3}K_{25}$ and $^{EG2}K_{25}$, with an emphasis on the side-chain urethane bond. Both free and hydrogen-bonded urethane were found for $^{EG2}K_{25}$ and $^{EG3}K_{25}$ in the solid state but with the former showing more intensive and ordered hydrogen bonding than the latter (Figure 5a). Ordered and dense side-chain hydrogen bonds play a crucial role in forming a stable β-sheet secondary structure in $^{EG2}K_n$, and molecular dynamics simulations have further proven this point. We investigated the interactions of $^{EG2}K_n$ in two models, namely, antiparallel (Figure 5b) and parallel β-sheets (Figure 5c). To elucidate interchain forces, we utilized a system with four peptide chains and a DP of 10. During the simulation, we initially imposed bond-distance constraints between the side-chain C═O and the neighboring chain N−H to promote hydrogen bond formation between the side chains of adjacent chains (Figure 5d). Then, the bond-distance constraints were released in the following molecular dynamics simulations. We analyzed the detailed secondary structure changes of individual chains during the simulations and further quantified conformational stability by analyzing the relative β-sheet content over time. For the antiparallel model, most of the residues in each chain remain in the yellow region throughout the simulation, corresponding to the extended and bridge structures, both of which represent β-sheets (Figure 5e). Additionally, the relative content of β-sheet in the antiparallel model ranges mostly between 65 and 80% (Figure 5f). These results suggest that $^{EG2}K_n$ maintains a stable β-sheet conformation during the simulation. Moreover, the parallel model also exhibits a relatively stable β-sheet secondary structure (Figure S16). However, the continuity of the yellow region (β-sheet) is not as pronounced for parallel structures, and the relative content of β-sheet fluctuates between 40 and 80% (Figure S17), indicating that the stability of the parallel model is weaker than that of the antiparallel model. This difference is likely due to the higher energetic favorability of antiparallel sheets over parallel sheets.[54] Since β-sheets are primarily stabilized by hydrogen bonds formed between the main chain's amide (N−H) and carbonyl (C═O) groups,[55] we quantified the number of hydrogen bonds between the main chains. The results indicate that the number of main chain hydrogen bonds for each pair of adjacent chains remains relatively stable, averaging around 4−6 for the antiparallel β-sheet (Figure 5g) and around 2−3 for the parallel β-sheet (Figure S18), indicating a relatively stable secondary structure. Hydrogen bonds can also form between the side chains of two units within the same chain and between units in different chains of $^{EG2}K_n$, which further supports the stability of the secondary structure and the self-assembly result. Therefore, in addition to the number of main-chain hydrogen bonds between different main chains, we also counted the number of side-chain hydrogen bonds between C═O and N−H, both between different chains and within the same chain. The number of hydrogen bonds between different chains is about 2−3 for the antiparallel β-sheet (Figure 5h) and about 1 for the parallel β-sheet (Figure S19), while the number of hydrogen bonds within the same chain is about 1−2 for the antiparallel β-sheet (Figure 5i) and about 2−4 for the parallel β-sheet (Figure S20). Overall, in addition to the hydrogen bonds of the main chain, the hydrogen bonds formed between the carbonyl oxygen and the amide hydrogen on the side chains also play a significant role in maintaining the β-sheet structure of these two molecules.

Taken together, we hypothesized that the side-chain urethane of $^{EG2}K_{25}$ facilitated the self-assembly and stabilized the β-sheet by generating extensive interchain hydrogen bonding. $^{EG3}K_{25}$, however, would nor favor the β-sheet as the side-chain EG_3 was too bulky. To reduce the steric hindrance/repulsion of EG_3, the backbone of $^{EG3}K_{25}$ thus preferred to form the single-stranded α-helix structure with a reduced side-chain density than the β-sheet (Figure S21). This side-chain repulsion of EG_3 would be more prominent in an aqueous solution than in a solid state when EG_3 bears a bulky hydration layer.

CONCLUSIONS

In summary, we reported a series of examples based on EG_m-modified poly-L-lysine. The solubility and secondary structures of the resulting polypeptides were governed not only by the length of EG_m but also by the DP of the polymer. Notably, an unusual nonionic water-soluble β-sheet polypeptide $^{EG2}K_{25}$ was obtained, which demonstrated a strong ability to form transparent, injectable, and self-healable hydrogels at a concentration as low as 1 wt %. The results of this work also highlighted the important role of the linkage unit in regulating secondary structures, as compared to previous works reporting very similar structures. The excellent water solubility and interesting self-assembly behavior make these polypeptides of great potential for various advanced biomedical applications.

ASSOCIATED CONTENT

Supporting Information

The Supporting Information is available free of charge at https://pubs.acs.org/doi/10.1021/acs.biomac.4c00759.

Full synthesis details of ^{EG1}K-NCA, ^{EG3}K-NCA, $^{EG1}K_n$, and $^{EG3}K_n$; experimental methods; characterizations; ^{1}H NMR, ^{13}C NMR, FT-IR, ESI-MS, and CD spectra; state of $^{EG2}K_{25}$ solution at different pH; XRD results; DLS curve of $^{EG2}K_{25}$; photograph of $^{EG1}K_{25}$ in deionized water; photograph of $^{EG3}K_{25}$ at different temperatures; secondary structure evolution; β-sheet content; total number of hydrogen bonds between main and side chains; and hypothetical diagram of the states of $^{EG2}K_{25}$ and $^{EG3}K_{25}$ (PDF)

AUTHOR INFORMATION

Corresponding Authors

Lijiang Yang − *Beijing National Laboratory for Molecular Sciences, College of Chemistry and Molecular Engineering, Peking University, Beijing 100871, China*; Email: yanglj@pku.edu.cn

Yiqin Gao − *Beijing National Laboratory for Molecular Sciences, College of Chemistry and Molecular Engineering, Peking University, Beijing 100871, China; Changping Laboratory, Beijing 102200, China;* orcid.org/0000-0002-4309-9376; Email: gaoyq@pku.edu.cn

Hua Lu − *Beijing National Laboratory for Molecular Sciences, Center for Soft Matter Science and Engineering, Key Laboratory of Polymer Chemistry and Physics of Ministry of Education, College of Chemistry and Molecular Engineering, Peking University, Beijing 100871, China;* orcid.org/0000-0003-2180-3091; Email: chemhualu@pku.edu.cn

https://doi.org/10.1021/acs.biomac.4c00759
Biomacromolecules 2024, 25, 5343−5351

Authors

Xiaodong Jing − *Beijing National Laboratory for Molecular Sciences, Center for Soft Matter Science and Engineering, Key Laboratory of Polymer Chemistry and Physics of Ministry of Education, College of Chemistry and Molecular Engineering, Peking University, Beijing 100871, China*

Zhen Zhu − *Changping Laboratory, Beijing 102200, China*

Shuo Wang − *Beijing National Laboratory for Molecular Sciences, Center for Soft Matter Science and Engineering, Key Laboratory of Polymer Chemistry and Physics of Ministry of Education, College of Chemistry and Molecular Engineering, Peking University, Beijing 100871, China;* orcid.org/0000-0002-1380-5890

Jiaqi Xin − *Beijing National Laboratory for Molecular Sciences, Center for Soft Matter Science and Engineering, Key Laboratory of Polymer Chemistry and Physics of Ministry of Education, College of Chemistry and Molecular Engineering, Peking University, Beijing 100871, China*

Haisen Zhou − *Beijing National Laboratory for Molecular Sciences, Center for Soft Matter Science and Engineering, Key Laboratory of Polymer Chemistry and Physics of Ministry of Education, College of Chemistry and Molecular Engineering, Peking University, Beijing 100871, China*

Letian Wang − *Beijing National Laboratory for Molecular Sciences, Center for Soft Matter Science and Engineering, Key Laboratory of Polymer Chemistry and Physics of Ministry of Education, College of Chemistry and Molecular Engineering, Peking University, Beijing 100871, China*

Huimin Tong − *Department of Instrument Analysis Center of Xi'an Jiaotong University, Xi'an 710049, China*

Chenhui Cui − *Department of Instrument Analysis Center of Xi'an Jiaotong University, Xi'an 710049, China*

Yanfeng Zhang − *Department of Applied Chemistry, School of Science, MOE Key Laboratory for Nonequilibrium Synthesis and Modulation of Condensed Matter (Xi'an Jiaotong University), Xi'an Key Laboratory of Sustainable Energy Materials Chemistry and State Key Laboratory for Mechanical Behavior of Materials, Xi'an Jiaotong University, Xi'an 710049, China;* orcid.org/0000-0003-4711-8690

Fei Sun − *Department of Chemical and Biological Engineering, the Hong Kong University of Science and Technology, Kowloon, Hong Kong 999077, China;* orcid.org/0000-0002-3065-7471

Complete contact information is available at: https://pubs.acs.org/10.1021/acs.biomac.4c00759

Author Contributions

[¶]Xiaodong Jing and Zhen Zhu contributed equally to this paper. Xiaodong Jing: investigation, software, data analysis, writing, and reviewing. Zhen Zhu: molecular dynamics simulation, data analysis, and writing. Shuo Wang: investigation and data analysis. Jiaqi Xin: data analysis. Haisen Zhou: data analysis. Letian Wang: data analysis. Huimin Tong, Chenhui Cui, and Yanfeng Zhang: cryo-TEM characterization. Fei Sun: data analysis. Lijiang Yang and Yiqin Gao: data analysis and reviewing. Hua Lu: conceptualization, methodology, project administration, reviewing, and funding acquisition.

Notes

The authors declare no competing financial interest.

■ ACKNOWLEDGMENTS

This work was supported by the National Natural Science Foundation of China (22125101), Beijing Natural Science Foundation (2220023), and Li Ge-Zhao Ning Life Science Youth Research Fund.

■ REFERENCES

(1) Duan, H.; Li, J.; Xue, J.; Qi, D. Metal-enhanced helical chirality of coil macromolecules: bioinspired by metal coordination-induced protein folding. *Biomacromolecules* **2023**, *24* (1), 344−357.

(2) Bonduelle, C. Secondary structures of synthetic polypeptide polymers. *Polym. Chem.* **2018**, *9* (13), 1517−1529.

(3) Gething, M. J.; Sambrook, J. Protein folding in the cell. *Nature* **1992**, *355*, 33−45.

(4) Liu, H.; Zhou, Y.; Liu, Y.; Wang, Z.; Zheng, Y.; Peng, C.; Tian, M.; Zhang, Q.; Li, J.; Tan, H.; Fu, Q.; Ding, M. Protein-inspired polymers with metal-site-regulated ordered conformations. *Angew. Chem., Int. Ed.* **2023**, *62* (6), No. e202213000.

(5) Ge, C.; Ye, H.; Wu, F.; Zhu, J.; Song, Z.; Liu, Y.; Yin, L. Biological applications of water-soluble polypeptides with ordered secondary structures. *J. Mater. Chem. B* **2020**, *8* (31), 6530−6547.

(6) Song, Z.; Han, Z.; Lv, S.; Chen, C.; Chen, L.; Yin, L.; Cheng, J. Synthetic polypeptides: from polymer design to supramolecular assembly and biomedical application. *Chem. Soc. Rev.* **2017**, *46* (21), 6570−6599.

(7) Deming, T. J. Synthesis of side-chain modified polypeptides. *Chem. Rev.* **2016**, *116* (3), 786−808.

(8) Zhang, Y.; Lu, H.; Lin, Y.; Cheng, J. Water-soluble polypeptides with elongated, charged side chains adopt ultrastable helical conformations. *Macromolecules* **2011**, *44* (17), 6641−6644.

(9) Gabrielson, N. P.; Lu, H.; Yin, L.; Li, D.; Wang, F.; Cheng, J. Reactive and bioactive cationic α-helical polypeptide template for nonviral gene delivery. *Angew. Chem., Int. Ed. Engl.* **2012**, *51* (5), 1143−1147.

(10) Song, Z.; Zheng, N.; Ba, X.; Yin, L.; Zhang, R.; Ma, L.; Cheng, J. Polypeptides with quaternary phosphonium side chains: Synthesis, characterization, and cell-penetrating properties. *Biomacromolecules* **2014**, *15* (4), 1491−1497.

(11) Zhang, R.; Zheng, N.; Song, Z.; Yin, L.; Cheng, J. The effect of side-chain functionality and hydrophobicity on the gene delivery capabilities of cationic helical polypeptides. *Biomaterials* **2014**, *35* (10), 3443−3454.

(12) Xiong, M.; Lee, M. W.; Mansbach, R. A.; Song, Z.; Bao, Y.; Peek, R. M.; Yao, C.; Chen, L. F.; Ferguson, A. L.; Wong, G. C. L.; Cheng, J. Helical antimicrobial polypeptides with radial amphiphilicity. *Proc. Natl. Acad. Sci. U.S.A.* **2015**, *112* (43), 13155−13160.

(13) Yuan, J.; Zhang, Y.; Sun, Y.; Cai, Z.; Yang, L.; Lu, H. Salt and pH triggered helix-coil transition of ionic polypeptides under physiology conditions. *Biomacromolecules* **2018**, *19* (6), 2089−2097.

(14) Zhang, C.; Yuan, J.; Lu, J.; Hou, Y.; Xiong, W.; Lu, H. From neutral to zwitterionic poly(α-amino acid) nonfouling surfaces: Effects of helical conformation and anchoring orientation. *Biomaterials* **2018**, *178*, 728−737.

(15) Hou, Y.; Zhou, Y.; Wang, H.; Sun, J.; Wang, R.; Sheng, K.; Yuan, J.; Hu, Y.; Chao, Y.; Liu, Z.; Lu, H. Therapeutic protein PEPylation: The helix of nonfouling synthetic polypeptides minimizes antidrug antibody generation. *ACS Cent. Sci.* **2019**, *5* (2), 229−236.

(16) Rodríguez-Hernández, J.; Lecommandoux, S. Reversible inside-out micellization of pH-responsive and water-soluble vesicles based on polypeptide diblock copolymers. *J. Am. Chem. Soc.* **2005**, *127* (7), 2026−2027.

(17) Nguyen, M.; Stigliani, J. L.; Pratviel, G.; Bonduelle, C. Nucleopolypeptides with DNA-triggered α helix-to-β sheet transition. *Chem. Commun.* **2017**, *53* (54), 7501−7504.

(18) Liu, Y.; Yin, L. α-Amino acid *N*-carboxyanhydride (NCA)-derived synthetic polypeptides for nucleic acids delivery. *Adv. Drug Delivery Rev.* **2021**, *171*, 139−163.

(19) Liu, Y.; Ren, Z.; Zhang, N.; Yang, X.; Wu, Q.; Cheng, Z.; Xing, H.; Bai, Y. A nanoscale MOF-based heterogeneous catalytic system for the polymerization of *N*-carboxyanhydrides enables direct routes toward both polypeptides and related hybrid materials. *Nat. Commun.* **2023**, *14* (1), 5598.
(20) Chen, C.; Fu, H.; Baumgartner, R.; Song, Z.; Lin, Y.; Cheng, J. Proximity-induced cooperative polymerization in "hinged" helical polypeptides. *J. Am. Chem. Soc.* **2019**, *141* (22), 8680−8683.
(21) Jiang, J.; Sun, H.; Wei, P.; Sun, M.; Lin, S.; Lv, M.; Fan, Z.; Zhu, Y.; Du, J. $\pi-\pi$ Interlocking Effect for Designing Biodegradable Nanorods with Controlled Lateral Surface Curvature. *Chem. Mater.* **2022**, *34* (11), 4937−4945.
(22) Kramer, J.; Deming, T. J. Glycopolypeptides with a Redox-Triggered Helix-to-Coil Transition. *J. Am. Chem. Soc.* **2012**, *134* (9), 4112−4115.
(23) Engler, A.; Lee, H.; Hammond, P. Highly efficient "grafting onto" a polypeptide backbone using click chemistry. *Angew. Chem., Int. Ed.* **2009**, *48* (49), 9334−9338.
(24) Carlsen, A.; Lecommandoux, S. Self-assembly of polypeptide-based block copolymer amphiphiles. *Curr. Opin. Colloid Interface Sci.* **2009**, *14* (5), 329−339.
(25) Deming, T. J. Preparation and development of block copolypeptide vesicles and hydrogels for biological and medical applications. *Wiley Interdiscip. Rev.: Nanomed. Nanobiotechnol.* **2014**, *6* (3), 283−297.
(26) Jing, X.; Hu, H.; Sun, Y.; Yu, B.; Cong, H.; Shen, Y. The intracellular and extracellular microenvironment of tumor site: The trigger of stimuli-responsive drug delivery systems. *Small Methods* **2022**, *6* (3), 2101437.
(27) Wang, H.; Su, H.; Xu, T.; Cui, H. Utilizing the Hofmeister Effect to Induce Hydrogelation of Nonionic Supramolecular Polymers into a Therapeutic Depot. *Angew. Chem., Int. Ed.* **2023**, *62* (43), No. e202306652.
(28) Wu, G.; Ge, C.; Liu, X.; Wang, S.; Wang, L.; Yin, L.; Lu, H. Synthesis of water soluble and multi-responsive selenopolypeptides via ring-opening polymerization of *N*-carboxyanhydrides. *Chem. Commun.* **2019**, *55* (54), 7860−7863.
(29) Yu, M.; Nowak, A. P.; Deming, T. J.; Pochan, D. J. Methylated mono- and diethyleneglycol functionalized polylysines: Nonionic, α-helical, water-soluble polypeptides. *J. Am. Chem. Soc.* **1999**, *121* (51), 12210−12211.
(30) Wang, J.; Gibson, M. I.; Barbey, R.; Xiao, S. J.; Klok, H. A. Nonfouling polypeptide brushes via surface-initiated polymerization of N^{ϵ}-oligo(ethylene glycol)succinate-$_{L}$-lysine *N*-carboxyanhydride. *Macromol. Rapid Commun.* **2009**, *30* (9−10), 845−850.
(31) Chen, C.; Wang, Z.; Li, Z. Thermoresponsive polypeptides from pegylated poly-$_{L}$-glutamates. *Biomacromolecules* **2011**, *12* (8), 2859−2863.
(32) Zhang, S.; Chen, C.; Li, Z. Effects of molecular weight on thermal responsive property of pegylated poly-$_{L}$-glutamates. *Chin. J. Polym. Sci.* **2013**, *31* (2), 201−210.
(33) Fu, X.; Shen, Y.; Fu, W.; Li, Z. Thermoresponsive oligo(ethylene glycol) functionalized poly-$_{L}$-cysteine. *Macromolecules* **2013**, *46* (10), 3753−3760.
(34) Ma, Y.; Fu, X.; Shen, Y.; Fu, W.; Li, Z. Irreversible low critical solution temperature behaviors of thermal-responsive OEGylated poly($_{L}$-cysteine) containing disulfide bonds. *Macromolecules* **2014**, *47* (14), 4684−4689.
(35) Tang, H.; Yin, L.; Lu, H.; Cheng, J. Water-soluble poly($_{L}$-serine)s with elongated and charged side-chains: synthesis, conformations, and cell-penetrating properties. *Biomacromolecules* **2012**, *13* (9), 2609−2615.
(36) Hwang, J.; Deming, T. J. Methylated Mono- and Di(ethylene glycol)-Functionalized β-Sheet Forming Polypeptides. *Biomacromolecules* **2001**, *2* (1), 17−21.
(37) Xiong, W.; Fu, X.; Wan, Y.; Sun, Y.; Li, Z.; Lu, H. Synthesis and multimodal responsiveness of poly(α-amino acid)s bearing OEGylated azobenzene side-chains. *Polym. Chem.* **2016**, *7* (41), 6375−6382.
(38) Xiong, W.; Zhou, H.; Zhang, C.; Lu, H. An amino acid-based gelator for injectable and multi-responsive hydrogel. *Chin. Chem. Lett.* **2017**, *28* (11), 2125−2128.
(39) Ge, C.; Liu, W.; Ling, Y.; Tang, H. Synthesis and thermoresponsive properties of OEGylated polypeptide with a LCST at body temperature in water and with a UCST in alcohol or ethanol/water solvent mixture. *J. Polym. Sci., Part A: Polym. Chem.* **2018**, *56* (2), 163−173.
(40) Zhang, C.; Lu, H. Helical nonfouling polypeptides for biomedical applications. *Chin. J. Polym. Sci.* **2022**, *40* (5), 433−446.
(41) Wang, J.; Zhou, P.; Shen, T.; Xu, S.; Bai, T.; Ling, J. Glycine *N*-thiocarboxyanhydride: a key to glycine-rich protein mimics. *ACS Macro Lett.* **2023**, *12* (11), 1466−1471.
(42) Nguyen, M.; Stigliani, J.; Bijani, C.; Verhaeghe, P.; Pratviel, G.; Bonduelle, C. Ionic Polypeptide Polymers with Unusual β-Sheet Stability. *Biomacromolecules* **2018**, *19* (10), 4068−4074.
(43) Wang, S.; Lu, H. Ring-opening polymerization of amino acid *N*-carboxyanhydrides with unprotected/reactive side groups. I. $_{D}$-Penicillamine *N*-carboxyanhydride. *ACS Macro Lett.* **2023**, *12* (5), 555−562.
(44) Tian, Z. Y.; Zhang, Z.; Wang, S.; Lu, H. A moisture-tolerant route to unprotected α/β-amino acid *N*-carboxyanhydrides and facile synthesis of hyperbranched polypeptides. *Nat. Commun.* **2021**, *12* (1), 5810.
(45) Quadrifoglio, F.; Urry, D. W. Ultraviolet rotatory properties of polypeptides in solution. II. Poly-L-serine. *J. Am. Chem. Soc.* **1968**, *90* (11), 2760−2765.
(46) Krebs, M. R. H.; Bromley, E. H. C.; Donald, A. M. The binding of thioflavin-T to amyloid fibrils: localisation and implications. *J. Struct. Biol.* **2005**, *149* (1), 30−37.
(47) Wang, S.; He, W.; Xiao, C.; Tao, Y.; Wang, X. Synthesis of Y-shaped OEGylated poly(amino acid)s: the impact of OEG architecture. *Biomacromolecules* **2019**, *20* (4), 1655−1666.
(48) Zhao, X.; Sun, H.; Zhang, X.; Ren, J.; Shao, F.; Liu, K.; Li, W.; Zhang, A. OEGylated collagen mimetic polypeptides with enhanced supramolecular assembly. *Polymer* **2016**, *99*, 281−291.
(49) Cheng, Y.; He, C.; Xiao, C.; Ding, J.; Zhuang, X.; Huang, Y.; Chen, X. Decisive role of hydrophobic side groups of polypeptides in thermosensitive gelation. *Biomacromolecules* **2012**, *13* (7), 2053−2059.
(50) Sun, Y.; Jing, X.; Liu, Y.; Yu, B.; Hu, H.; Cong, H.; Shen, Y. A chitosan derivative-crosslinked hydrogel with controllable release of polydeoxyribonucleotides for wound treatment. *Carbohydr. Polym.* **2023**, *300*, 120298.
(51) Wu, Q.; Hu, Y.; Yu, B.; Hu, H.; Xu, F. J. Polysaccharide-based tumor microenvironment-responsive drug delivery systems for cancer therapy. *J. Controlled Release* **2023**, *362*, 19−43.
(52) Geng, C.; Wang, S.; Wang, H. Recent advances in thermoresponsive OEGylated poly(amino acid)s. *Polymers* **2021**, *13* (11), 1813.
(53) Huang, J.; Heise, A. Stimuli responsive synthetic polypeptides derived from N-carboxyanhydride (NCA) polymerisation. *Chem. Soc. Rev.* **2013**, *42*, 7373−7390.
(54) Zhao, L.; Wu, Y. D. A theoretical study of beta-sheet models: is the formation of hydrogen-bond networks cooperative. *J. Am. Chem. Soc.* **2002**, *124* (8), 1570−1571.
(55) Pauling, L.; Corey, R. B. The pleated sheet, a new layer configuration of polypeptide chains. *Proc. Natl. Acad. Sci. U.S.A.* **1951**, *37* (5), 251−256.

https://doi.org/10.1021/acs.biomac.4c00759
Biomacromolecules 2024, 25, 5343−5351